EDSU Journal of Engineering and Technology (EDSUJET) Vol. 2 (1), pp. 199 – 220. 2026
ISSN (Print):3121 – 8725 eISSN (Online): 3121 – 8597


# COMPUTATIONAL FLUID DYNAMICS OF VEHICLE GEOMETRY BY REDUCING DRAG FORCE IN ANSYS

Abu Jonathan Unuakhenah[a],* and Festus Oamen Isaac[b]

[a] Department of Mechanical Engineering, Edo State University Iyamho. Edo State, Nigeria.
[b] Department of Mechanical Engineering, Edo State University Iyamho. Edo State, Nigeria.

*Corresponding Author Email: joeunuakhenahbua@gmail.com

**Received**: 14 November 2025, **Accepted**: 19 February 2026, **Published**: 31 March 2026

**K E Y W O R D S**

Toyota Hiace 2024, SolidWorks 2023, Computational fluid dynamics (CFD), ANSYS Fluid Flow (CFX), Drag force, aerodynamic analysis.

**A B S T R A C T**

In this paper, the aerodynamic analysis by varying different air speeds and considering the variation of aerodynamic properties as they affect vehicle drag forces in two different road vehicle models was carried out. The methodology implies importing the models, respectively, into the ANSYS Workbench for the computational fluid dynamics (CFD) analysis using the ANSYS Fluid Flow (CFX) tool. The optimized model had a spoiler added at the rear top of the conventional one. The findings showed that the optimized Toyota Hiace model highly outperformed and produced better results than the conventional one. The drag forces and static pressures of the optimized Hiace model were drastically reduced to enhance vehicle fuel economy, stability and high performance. The drag force at an air speed of 40 m/s for the conventional model was -2741.77 N and -2241.18 N for the optimized one. Literature has it that a well-optimized aerodynamic design reduces air resistance (drag force), which is one of the most dominant forces acting against a moving vehicle. Detailed results obtained at speeds of 45 m/s and 50 m/s, respectively, are shown in the results section of this paper.

## 1. INTRODUCTION

Computational fluid dynamics (CFD) represents a crucial aspect of fluid mechanics that employs numerical methods, techniques and algorithms to make deductions and analysis on the complexities found in fluid flow concepts (Ainul et al, 2023). This field leverages the computational strength of modern computing systems and software to simulate and resolve the vital interaction between fluids and solid boundaries set in operation within a constrained boundary (Nath et al, 2021). Through the computational ability of these high-performance supercomputers via design software, researchers are continuously on a drive to enhance the

precision and efficiency of CFD simulations, particularly in the contexts of transonic or turbulent flow. The process of validating CFD software results typically commences with preliminary evaluations conducted within wind tunnel settings, followed by extensive real-world assessments that end with field testing. In the field of fluid dynamics and a large expanse of other fields of discipline, CFD stands as an indispensable instrument alongside empirical and theoretical methods employed for resolving simulation and modelling problems (Ainul et al, 2023). Having evolved from conventional techniques like potential flow analysis and boundary-layer theory, computational fluid dynamics now has influence in various fields that include engineering, physics, chemistry, meteorology, and geology. The foundational constituents of CFD, as propounded by (John, 2009), occupy a central position in its application and evolution aimed at capturing fluid behaviour and its interactions with bodies in motion (Nath et al, 2021). The importance of CFD as it concerns Nigeria cannot be overemphasized because it enables one to know the geometry of road and flight vehicles, which would help to reduce drag forces and encourage down forces (Nur and Mohammad, 2024).

Garg (2019) reviewed Passive Drag Reduction Techniques for Vehicle Aerodynamics in his study. The study used ANSYS FLUID FLOW (CFX) CFD simulations to examine passive drag reduction strategies for enhancing vehicle aerodynamics. The evaluation of airflow over a vehicle and the impact of different devices on lift and drag coefficients were the main objectives of the study. The research compares several aerodynamic alterations made to the base model car using the realizable k-ε turbulence model. The findings demonstrated how these passive methods greatly impact wake creation, improve fluid flow, and lessen air recirculation, all of which minimize drag and improve aerodynamic efficiency (Garg, 2019). Muhammad et al. (2021) reviewed the aerodynamic influence on a car geometry by using the CFD techniques. This study employed CFD techniques to investigate the design features and application of many reference models to solve drag problems. In order to improve car performance and stability, the study examines the advantages and disadvantages of various models as well as the validity of the results. Its cost-effectiveness, shorter simulation times, and effective simulation results demonstrate the benefits of simplified generic models over specific car geometries. For precise and cost-effective CFD simulations in vehicle aerodynamics, the study emphasizes the need to choose suitable turbulence models (Muhammad Nabil Farhan Kamal et al., 2021). Ainul et al. (2023) carried out a CFD simulation of an aerodynamic truck using a cylinder as a drag reduction device. The impact of the cylinder on the truck's drag force was estimated numerically in this study by using ANSYS FLUID FLOW (CFX) CFD software. The study compared trucks with and without a cylinder above the head, trucks with windscreens, and trucks with different types of cylinders: round, type-I, and type-D cylinders. Using the k-epsilon turbulence model, the study was performed in a simulation at a speed of 30 m/s. In order to reduce errors and maximize iteration time, a grid independence test was performed.

The results of the simulation demonstrated that the truck's drag coefficient could be decreased by replacing the windscreen with round, I-type and D-type cylinders; the D-type cylinder achieved the largest reduction in drag coefficient, measuring 0.72. Therefore, by utilizing a D-type cylinder, changes to the drag reduction cylinder's design can indirectly reduce fuel usage by 69.5% (Ainul et al, 2023). Arabaci and Pakdemirli (2023) did a thorough examination into

the aerodynamic improvements of buses inspired by beluga whales. This study produced creative bus designs that drew inspiration from "whales". Only the frontal portion of the buses was covered with the designs. The new versions are called Beluga buses, and other model variations are all meant to resemble Beluga whales. To find the drag coefficients of different models, both experimental and numerical analyses were done. The numerical calculations were conducted using the ANSYS CFD programme. The drag coefficients were experimentally determined during wind tunnel tests. Results of computational fluid dynamics (CFD) were shown for the Beluga and Neoplan Skyliner models. Initially, the drag coefficient of the Sky. The model was computed using the finite volume approach to verify the accuracy of the computations. The computations produced a somewhat lower value of 0.392 than the manufacturer's specified drag coefficient of 0.41, showing strong agreement between the CFD results and the supplied data. At low Reynolds numbers, there is a 6.4% difference in the drag coefficients between the experimental and numerical results; at higher Reynolds numbers, this difference disappears. Hence, it was anticipated that the improved geometry would provide a cost-effective way to lower gasoline usage (Arabaci and Pakdemirli, 2023). Finally, very recent studies by Qin, Ricci and Blocken (2024) reviewed the numerical and experimental investigations of the DrivAer Model. The study made use of the DrivAer model, a generic car body, to undertake both computational and experimental experiments focusing on vehicle aerodynamics. A 1:4 scale DrivAer notchback model was used for CFD simulations and wind-tunnel testing by the researchers. The goal of the study was to investigate how alternative turbulence models and numerical techniques, in addition to surface grid resolution, prism layer heights, cell types, and downstream and upstream distances, affected the precision of the drag and lift coefficients. The results showed that the hybrid RANS-LES approach is a useful technique for simulating aerodynamic forces in automotive aerodynamics because it strikes a good balance between computing cost and accuracy (Qin et al., 2024). Ikrami et al. (2023) did a CFD analysis on a truck in order to improve its aerodynamic behaviour. They reduced the drag coefficient from 0.830 to 0.728 to get 12.29 % reduction in their study. However, in this study, a reduction from 0.9656 to 0.7488 to get 22.45 % reduction and 55.19 % increase in lift coefficient were recorded. Rutuja (2024) carried out a CFD analysis on a transport bus in order to improve its aerodynamic behaviour. He reduced the drag coefficient from 0.9 to 0.6 to get 33 % reduction, which was higher than the percentage reduction obtained in this study.

Having considered the work of previous researchers, it was noted that the reduction of drag force to improve the fuel economy and stability by using different road and flight vehicles was done without considering the increase of the lift force, especially the negative lift force. It was also noted that recent road vehicle models were not used in their findings. However, lift force acts perpendicularly to the motion of the object and results from pressure differences on a vehicle's upper and lower surfaces as it moves through air. Positive lift is undesirable as it reduces tyre grip, while negative lift (downforce) enhances road holding (Heisler, 2002; Nur and Mohammad, 2024). Nath, Pujari, Jain and Rastogi (2021) discussed the effects of different aerodynamic devices on the lift force. The results show that the lift force increases exponentially with the increase in speed. Drag force is a major setback when it comes to achieving high speeds in a moving vehicle. Velagapudi et al. (2015) improved the geometry of a car for a better flow around the model and a lower drag coefficient.

In this study, recent vehicle models would be considered in analyzing the interaction of moving air over, across and under vehicles. The aim was to improve the aerodynamic performance by reducing the drag force and coefficient through optimization of vehicle geometry using CFD simulations. The reduction of the drag force, drag coefficient and increase the lift force and lift coefficient would be possible by adding a rear spoiler made of a better airfoil to one of the models in this study.

## ii. MATERIALS AND METHODS

### 2.1 Materials

In aerodynamics, air is treated as a fluid, and its properties and behaviour are crucial for understanding how objects move through it, particularly in car/flight. Air's density, dynamic viscosity, and compressibility influence forces like lift and drag, which are fundamental to vehicles/ aircraft design and performance. The density of the air at 25°C with standard atmospheric pressure is $1.225\ kg/m^3$ and its dynamic viscosity is given as $1.7894\ x\ 10^{-5}\ kg/ms$.

### 2.2 Methods

The following methods would be applied in this study:

a) Modelling of the Toyota Hiace Bus 2024 and the optimized models, respectively, in the SolidWorks 2023 software after obtaining the vector drawings from www.the-blueprints.com;
b) Importing the models into ANSYS 2023 commercial software and creating enclosures called virtual wind tunnels, respectively, around the vehicle models, which would act as the air domains for the aerodynamics simulation of the air flow around and over them;
c) Meshing of the boundary layers of the enclosures to generate nodes and elements and applying the analysis model called viscous laminar and boundary conditions, which mainly comprises the inlet air at assumed speeds of $144\ (km/h)\ [40\ m/s]$, $162\ (km/h)\ [45\ m/s$ and $180\ (km/h)\ [50\ m/s]$, outlet gauge pressure of the virtual wind tunnel, air density, air kinematic viscosity, air room temperature, air atmospheric pressure, etc.;
d) Establishing the aerodynamic performance parameters of lift and drag forces/coefficients of the standard outer body shape of the models by simulating suitable aerodynamic conditions around the models in commercial Computational Fluid Dynamics (CFD) software called ANSYS FLUID FLOW (CFX);
e) Repeating the aerodynamic performance parameter measurements under optimized aerodynamic conditions in ANSYS FLUID FLOW (CFX) after attaching suitable aerodynamic (spoilers or wings) to the models;
f) Getting the velocity streamlines, vectors and pressure contours (static pressure) in the flow fields generated in each case to determine the causes for the variation in the values of the aerodynamic performance parameters of lift and drag coefficients measured;
g) Comparing the results of the simulation and determining the most aerodynamically efficient model through the various simulated drag and lift forces/coefficients, respectively.

### 2.2.1 Geometry Models

The Toyota Hiace Bus 2024 model was modelled in the SolidWorks 2023 software after obtaining the vector drawings from www.the-blueprints.com. See Fig. 1 for the vector drawings.

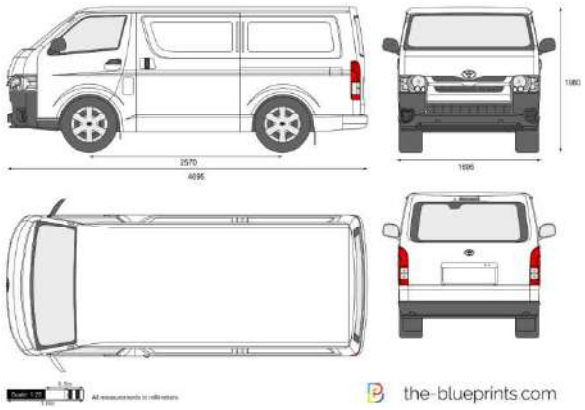


**Fig. 1**. Vector drawings of Toyota Hiace model

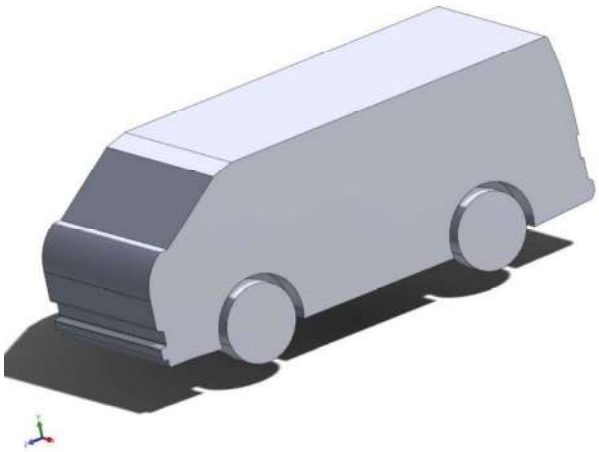

Fig. 2. Toyota Hiace model in SolidWorks

However, the above vector drawings for the vehicle were modelled in SolidWorks 2023 software, which would enable the Fluid Flow (CFX) analysis in ANSYS 2023 commercial software. Fig. 2 shows the model.

### 2.2.2 Importation of Models into ANSYS Software

The model was imported into ANSYS for the computational fluid dynamics (CFD) or aerodynamics analysis using the Fluid Flow (Fluent) application. See Figs 3 and 4. Thereafter, the creation of the virtual wind tunnel (enclosure) or Fluid Domain was done in the ANSYS Workbench DesignModeler after editing the models imported from the SolidWorks software.

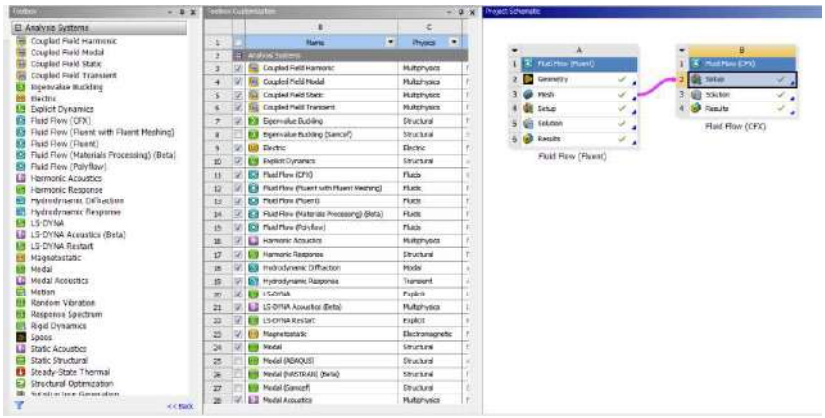

**Fig. 3.** ANSYS workbench GUI for the Fluid Flow (CFX) analysis

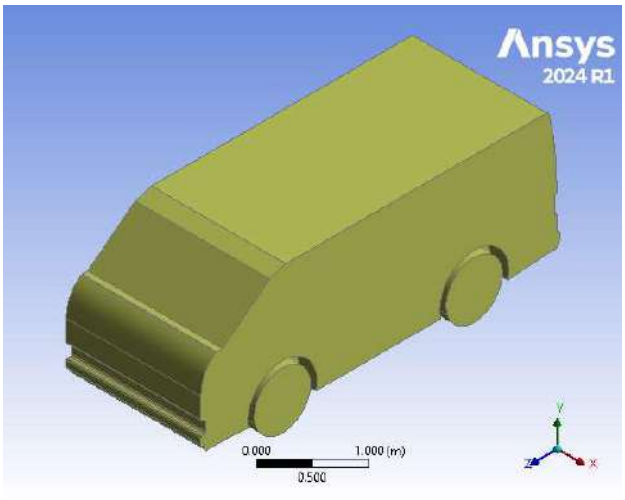


**Fig. 4.** Toyota Hiace model in ANSYS

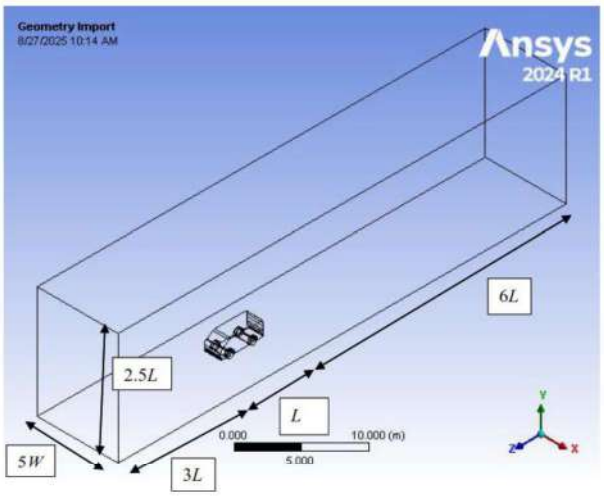


**Fig. 5.** Fluid Domain for the Toyota model

The boundary conditions at the front and top planes were named as velocity inlets with assumed incoming free stream air velocities or speeds as 144 $(km/h)$ [40 $m/s$], 162 $(km/h)$ [45 $m/s$, and 180 $(km/h)$ [50 $m/s$]. The rear plane was named the pressure outlet. The distance between the upstream velocity inlet and the models was $3L$. The pressure outlet, which was at a distance of $6L$ from the models was fixed at atmospheric pressure. The upstream velocity inlet and pressure outlet were defined with $5W$ by $2.5L$ of the models, respectively. The outer walls of the domain were also considered as a velocity inlet with the same velocity as the primary inlet. See Fig. 5.

### 2.2.3 Setup in CFX Pre-Processing

The boundary conditions within the CFX Pre-Processing included the inlet, outlet, walls (driver side, passenger side, top), road and car body. See Fig. 6.

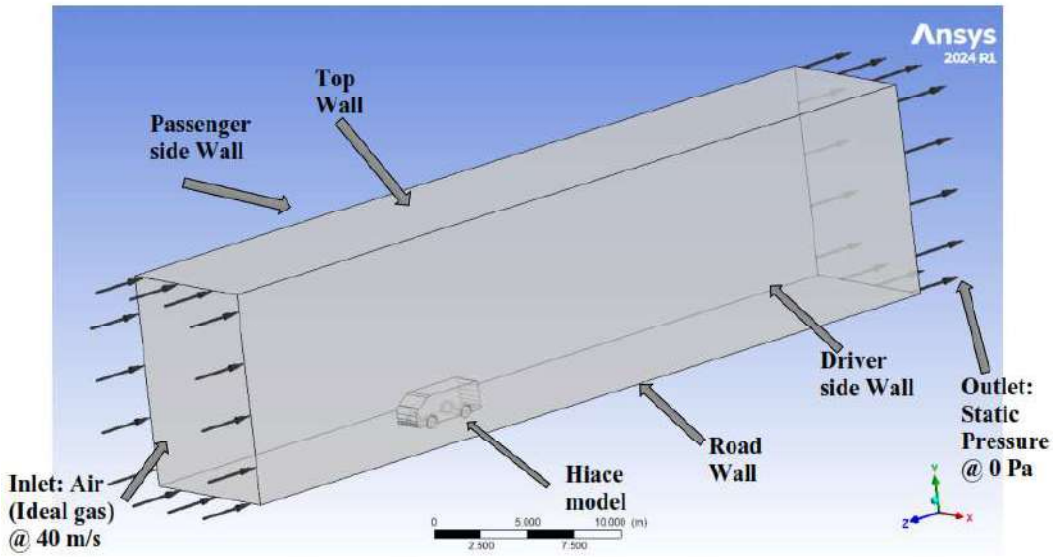


**Fig. 6.** Setup of the virtual wind tunnel with the Hiace model in CFX Pre-processing

Air inlet velocities or speeds of 40 m/s (144 km/h), 45 m/s (162 km/h) and 50 m/s (180 km/h) were used for the simulations. Theoretically, the drag coefficient is not dependent on the speed of the air; however, the Hiace model is expected to have the same drag coefficient ($C_d$) at any speed (Johan, 2013). As the velocity of the air increases, so does the drag, which is accounted for in the $C_d$ equation. Fluid models are mathematical models used in software packages like the ANSYS Fluid Flow (CFX) to simulate the flow of fluid for a specific scenario. Different types of fluid models are used for different types of analysis in computational fluid dynamics (CFD). Two of the commonly used fluid models for air flow are the k-Epsilon and Shear Stress Transport (SST). The k-Epsilon is a standard fluid model that can be used for a wide range of simulations (ANSYS Academic Research Release 14.5). The Shear Stress Transport (SST) fluid model is recommended for accurate boundary layer simulations (ANSYS Academic Research Release 14.5). For this study, which involves the aerodynamic properties of different road vehicles, the air flow at the boundaries is very important, and for this reason, the Shear Stress Transport (SST) model was used.

The common forms of the drag and lift equations (Stone, Richard and Ball) can be used for many different vehicles. These include cars, trucks, trains and motorbikes as the same principles apply.
The drag force ($F_D$) equation is given by:

$$F_D = \frac{1}{2} C_D \rho A_f V^2 \quad (1)$$

The drag coefficient equation is:

$$C_D = \frac{2F_D}{\rho A_f V^2} \quad (2)$$

Similarly, the lift force ($F_L$) equation is given by:

$$F_L = \frac{1}{2} C_D \rho A_f V^2 \quad (3)$$

The lift coefficient equation is:

$$C_L = \frac{2F_L}{\rho A_f V^2} \quad (4)$$

Where:
$\rho =$ Density of inlet air at a specified temperature $(1.225\ kg/m^3)$
$A_f =$ Frontal area of the models
$V^2 =$ Velocity of the air $(40\ m/s\ -60\ m/s)$
$C_D =$ Drag coefficient
$C_L =$ Lift coefficient

However, the frontal areas of the models were determined by using the SolidWorks software. See Fig. 7.
The frontal area of the optimized Hiace model was also measured as $(3.0545\ m^2)$.

### 2.2.4 Meshing of the Fluid Domains

Figure 8 shows the mesh Fluid Domains for the model. The meshing resulted in 160371 nodes and 868405 elements for the Hiace model and 87023 nodes and 461547 elements for the optimized Hiace model, as shown in Fig. 14.

The summary of the computational fluid dynamics (CFD) by using the Fluid Flow (CFX) Analysis System is shown in a flowchart in Fig. 9.

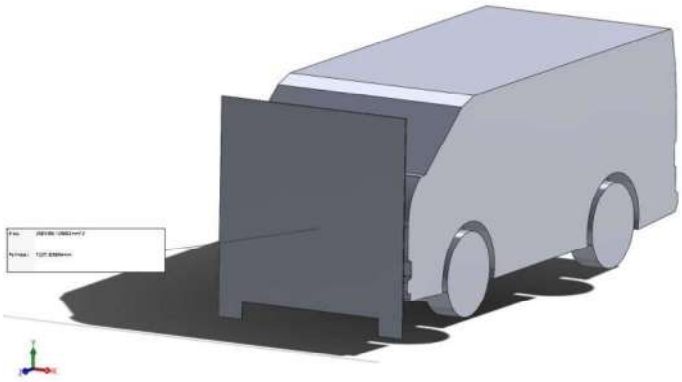

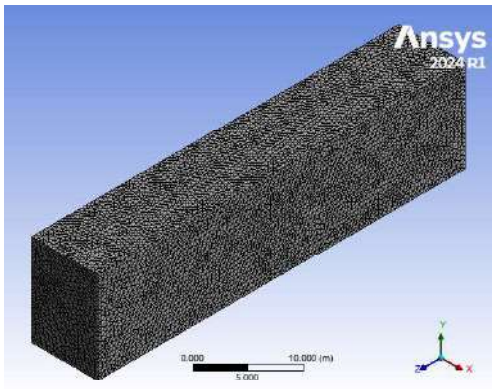


**Fig. 7**. Frontal area of the Hiace model ($2.905\ m^2$) Fig. 8. Meshed domain for Hiace model

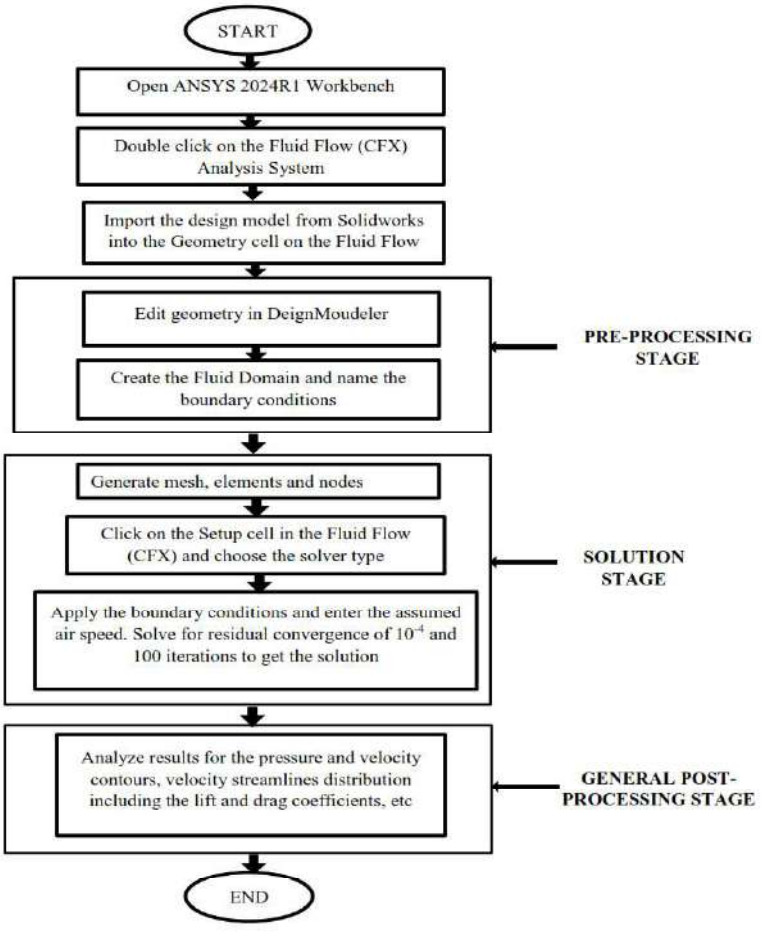


**Fig. 9.** Flowchart of the computational fluid dynamics using ANSYS Fluid Flow (CFX) ***(Source: Isaac and Abu, 2022)***

### 2.2.5 Optimization of the Toyota Hiace Bus by Attaching a Spoiler at the Top Rear

#### 2.2.5.1 Modelling of the Spoiler

The rear spoiler was modelled according to specifications given by Giguere and Selig (1997). The spoiler was modelled in SolidWorks by using the airfoil made by Giguere and Selig (1997). Fig. 10 shows the airfoil shape while, Fig. 11 is a CAD model of the completed rear spoiler. The coordinates and specifications of the SG airfoil were obtained from www.airfoiltools.com. The $x - y$ coordinates were used in the SolidWorks CAD software to create the geometry for the spoiler model.

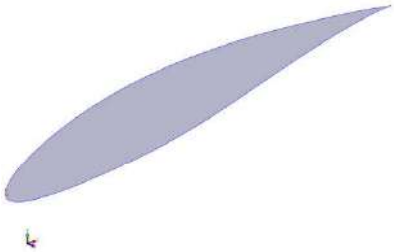

**Fig. 10.** SG6040 airfoil geometry

**Fig. 11.** Modelled spoiler for the optimized model

**Fig. 12.** The optimized Hiace model

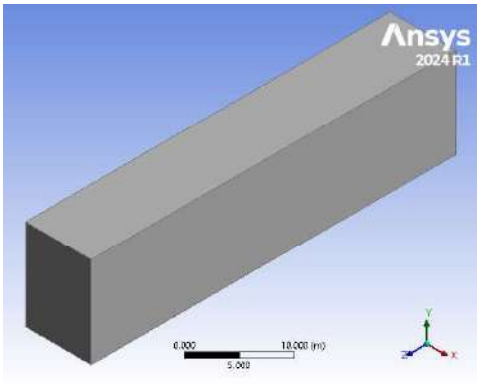


**Fig. 13.** Fluid Domain for the optimized Hiace model

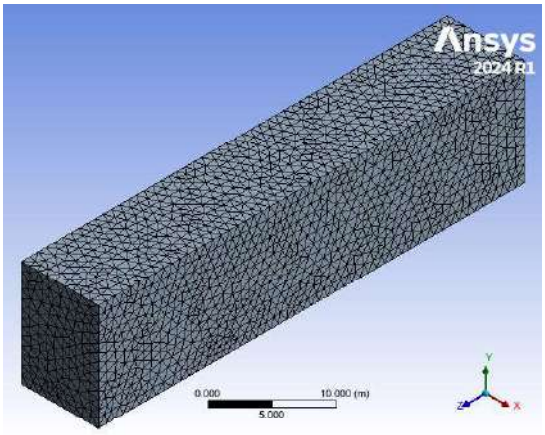


**Fig. 14.** Meshed view of the Fluid Domain with the optimized Hiace model

**Table 1**. Specification of the HP Laptop

| S/N | Description | Capacity |
|---|---|---|
| 1 | Ram | 8.00 GB |
| 2 | Processor | Intel (R) Celeron (R) CPU N3060 @ 1.60 GHz |
| 3 | Graphics Card | 114 MB |
| 4 | Storage | 466 GB |

Meanwhile, the specifications of the HP Laptop are shown in Table 1. Similarly, the time taken for each simulation for results based on the assumed wind speed is 60 secs.

## 3. RESULTS AND DISCUSSION

### 3.1 Results of the Conventional Toyota Hiace Model

The contour plots of the results obtained during the ANSYS Fluid Flow (CFX) post-processing of the conventional Toyota Hiace model for the air velocities or speeds of 144 $(km/h)$ [40 $m/s$], 162 $(km/h)$ [45 $m/s$ and 180 $(km/h)$ [50 $m/s$] are shown in Figs. 15 – 29. The CFX post-processing numerical values of the drag and lift forces are also shown.

At a speed of $V = 144\ km/h$ (40 $m/s$):

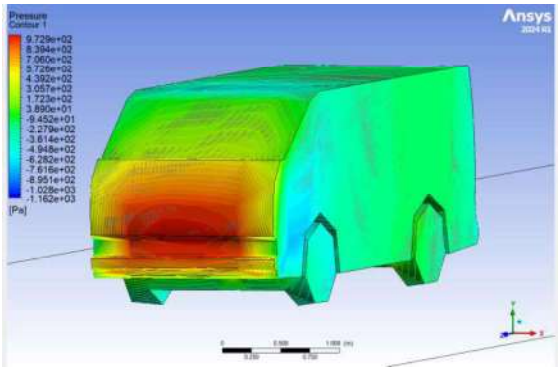


**Fig. 15.** Static pressure

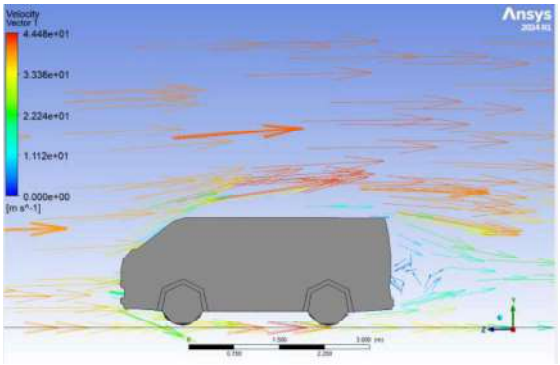


**Fig. 16.** Velocity vector

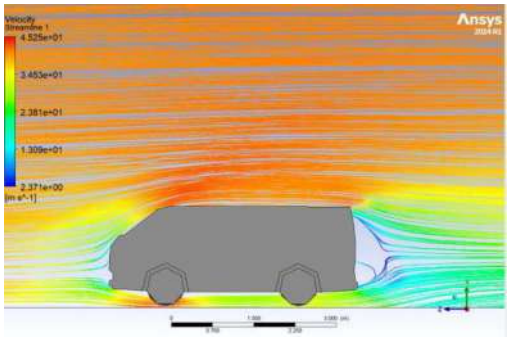


**Fig. 17.** Velocity streamlines

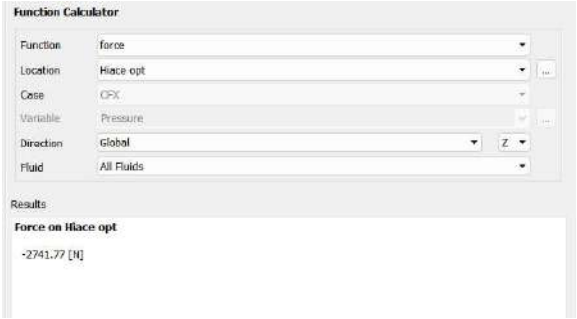


**Fig. 18.** Numerical drag force

The numerical drag force of the conventional Toyota Hiace model at 40 m/s is shown in Fig. 18. Similarly, the numerical lift force of the conventional Toyota Hiace model at 40 m/s is shown in Fig. 19.


**Fig. 19.** Numerical lift force of the conventional Toyota Hiace model at 40 m/s

At a speed of $V = 162\ (km/h)\ [45\ m/s]$:

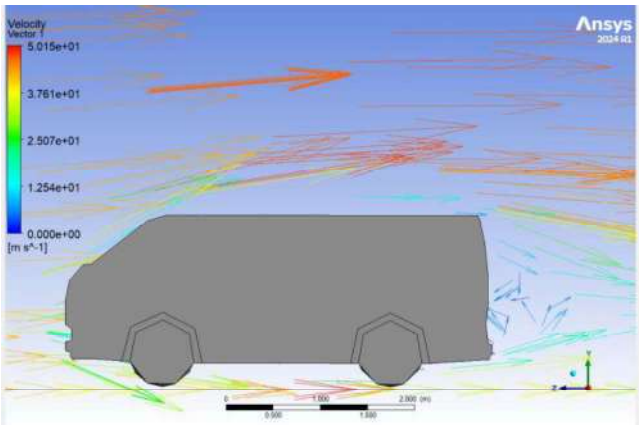


**Fig. 20.** Velocity vector

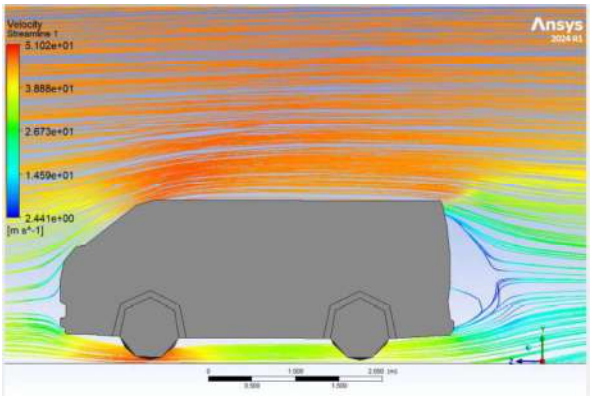


**Fig. 21.** Velocity streamlines

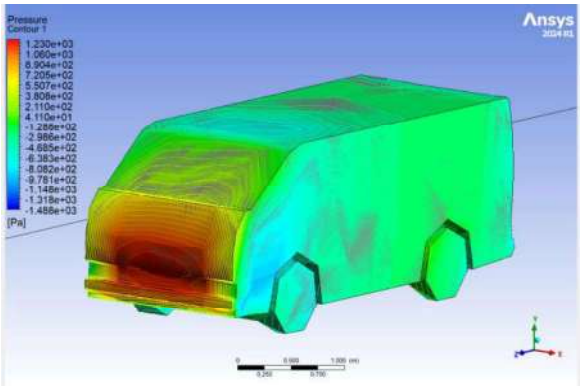


**Fig. 22.** Static pressure

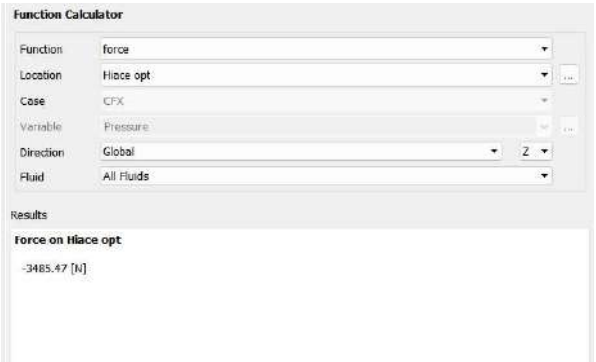


**Fig. 23.** Numerical drag force

The numerical drag force of the conventional Toyota Hiace model at 45 m/s is shown in Fig. 23. Similarly, the numerical lift force of the conventional Toyota Hiace model at 45 m/s is shown in Fig. 24.


**Fig. 24.** Numerical lift force of the conventional Toyota Hiace model at 45 m/s

At a speed of $V = 180\ km/h\ (50\ m/s)$:

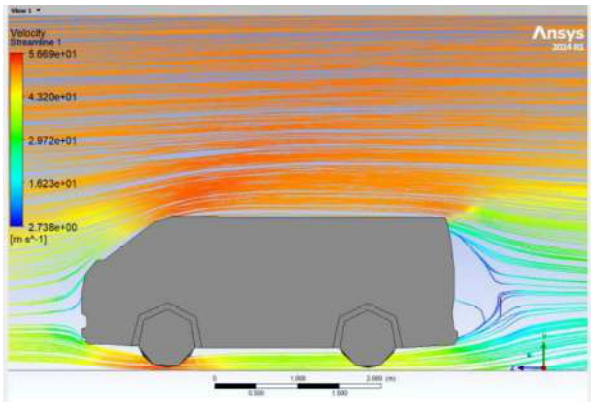


**Fig. 25.** Velocity streamlines

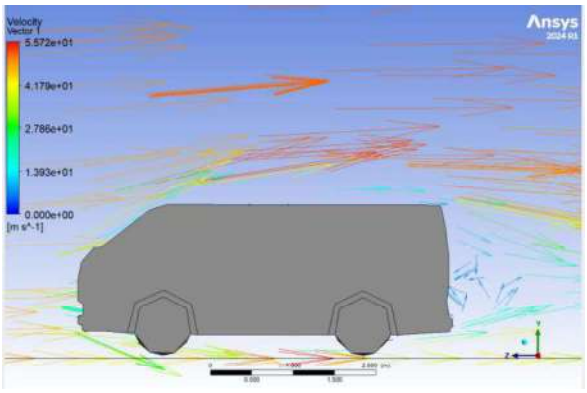


**Fig. 26.** Velocity vector

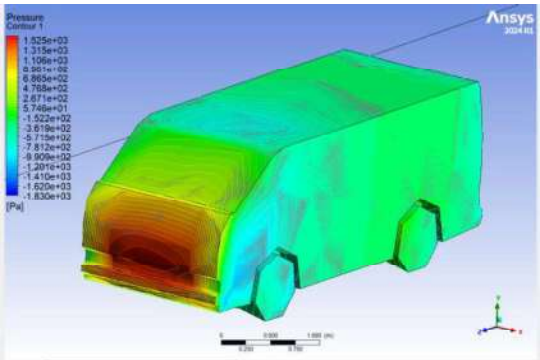


**Fig. 27.** Static pressure

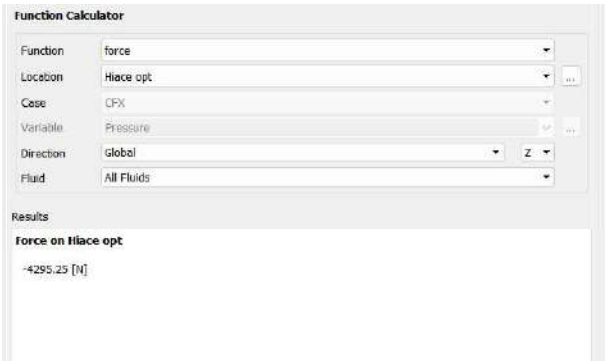


**Fig. 28.** Numerical drag force

The numerical drag force of the conventional Toyota Hiace model at 50 m/s is shown in Fig. 28. Similarly, the numerical lift force of the conventional Toyota Hiace model at 50 m/s is shown in Fig. 29.


**Fig. 29.** Numerical lift force of the conventional Toyota Hiace model at 50 m/s

The numerical values of the drag and lift forces were applied to Eqs. (1) – (4) to get the numerical drag and lift coefficients, respectively.

From the contour plots, numerical drag and lift forces for the specified wind speeds of 40 m/s, 45 m/s and 50 m/s shown in Figs. 15 – 29, it is seen that the conventional Toyota Hiace model exhibits high pressure at its front or nose in all the speeds of the air in the virtual wind tunnel. This is noted in the pressure contour (static pressure) plots. However, it was also seen from the colour legend bar that the static pressure increases as the speed of the air increases. This showed an increase in air resistance. Conversely, the minimum pressure occurs on the upper surfaces of the model, thereby contributing to the lift forces. Moreover, the CFX analysis gave negative drag and lift forces. The negative drag forces at all the wind speeds result from the direction of motion of the wind since it acts in the opposite direction in the Z-coordinate. Lift force acts perpendicular to the motion and results from pressure differences on a vehicle's upper and lower surfaces as it moves through the air. Positive lift is undesirable as it reduces tyre grip, while negative lift (downforce) enhances road holding (Heisler, 2002; Nur and Mohammad, 2024).
Table 2 shows the summary of the results from Figs. 15 – 29.

**Table 2.** Aerodynamic Properties of the Conventional Hiace Model

| **Speed (m/s)** | **Drag Coefficient $(C_D)$** | **Lift Coefficient $(C_L)$** | **Drag Force, $(F_D)$ (N)** | **Lift Force $(F_L)$ (N)** | **Maximum Static Pressure $(Pa)$** | **Maximum Velocity Streamline $(m/s)$** |
|---|---|---|---|---|---|---|
| 40 | 0.9631 | 0.3443 | -2741.77 | -980.211 | 972.9 | 45.25 |
| 45 | 0.9674 | 0.3480 | -3485.47 | -1253.95 | 1230 | 51.02 |
| 50 | 0.9656 | 0.3486 | -4295.25 | -1550.71 | 1525 | 56.69 |

Table 2 was used in plotting the graphs in Figs. 30 – 32.
From the Table and graphs for the specified wind speeds of 40 m/s, 45 m/s and 50 m/s as shown in Table 2 and Figs. 30 – 32. It is seen that the drag and lift coefficients appear to be approximately the same regardless of the wind speed. This shows that the drag and lift coefficients are not dependent on the speed of the air. Hence, the Hiace model is expected to have the same drag coefficient $(C_D)$ and lift coefficient $(C_L)$ at any speed (Johan, 2013). Similarly, it is also seen that the drag forces, lift forces, static pressures, and velocity streamlines of the conventional model increase as the wind speed increases.

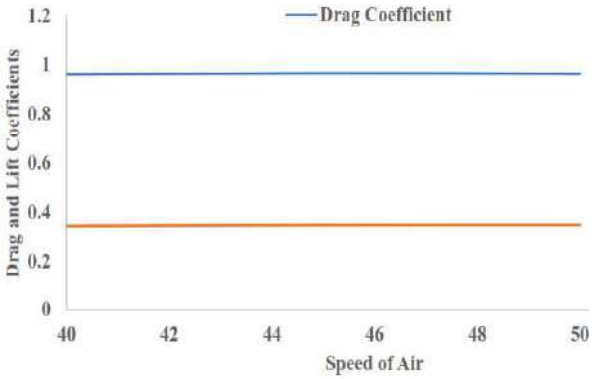


**Fig. 30.** Speed with drag and lift coefficient

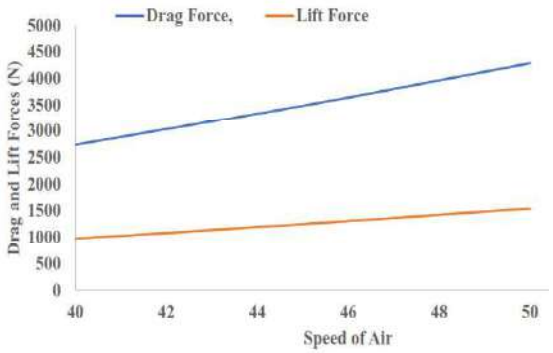


**Fig. 31.** Speed with drag and lift forces

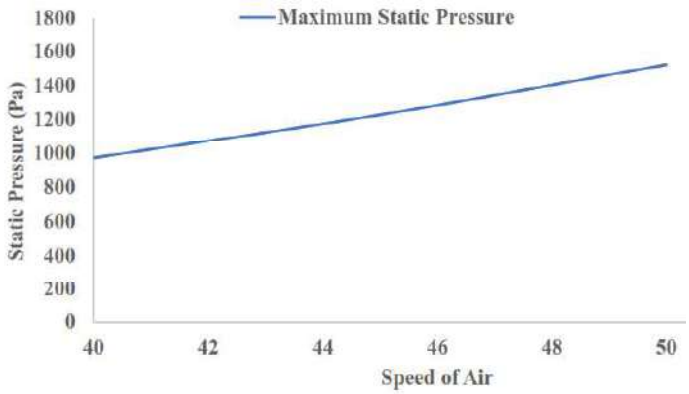


**Fig. 32.** Variation of speed with static pressure in the conventional Hiace model

### 3.2 Results of the Optimized Toyota Hiace Model

The contour plots of the results obtained during the ANSYS Fluid Flow (CFX) post-processing of the conventional optimized Toyota Hiace model for the air velocities or speeds of 144 $(km/h)$ [40 $m/s$], 162 $(km/h)$ [45 $m/s$ and 180 $(km/h)$ [50 $m/s$] are shown in Figs. 33 – 47. The CFX post-processing numerical values of the drag and lift forces are also shown.

At a speed of $V = 144\ km/h$ (40 $m/s$):

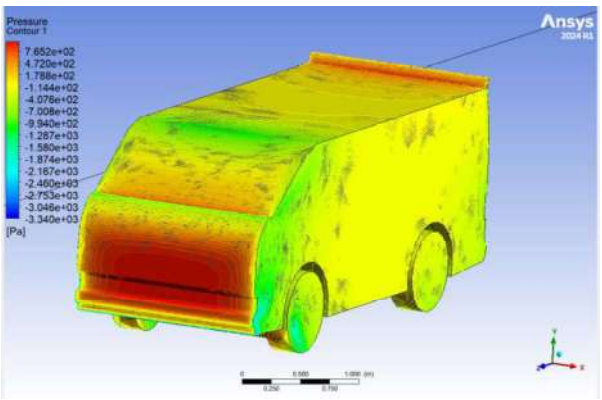


**Fig. 33.** Static pressure

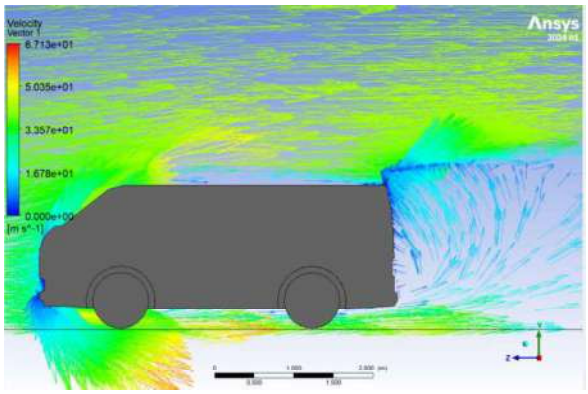


**Fig. 34.** Velocity vector

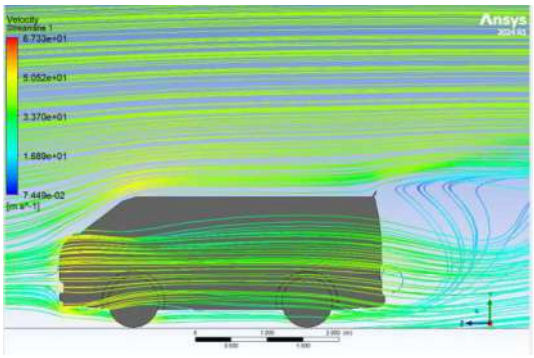


**Fig. 35.** Velocity streamlines

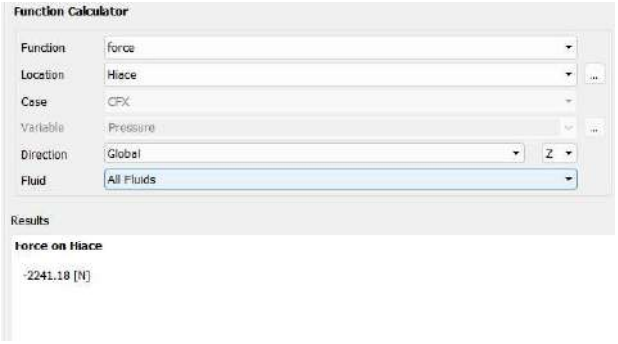


**Fig. 36.** Numerical drag force

The numerical drag force of the optimized Hiace model at 40 m/s is shown in Fig. 36. Similarly, the numerical drag force of the optimized Hiace model at 40 m/s is shown in Fig. 37.


**Fig. 37.** Numerical lift force of the optimized Hiace model at 40 m/s

At a speed of $V = 162\ km/h$ $(45\ m/s)$:

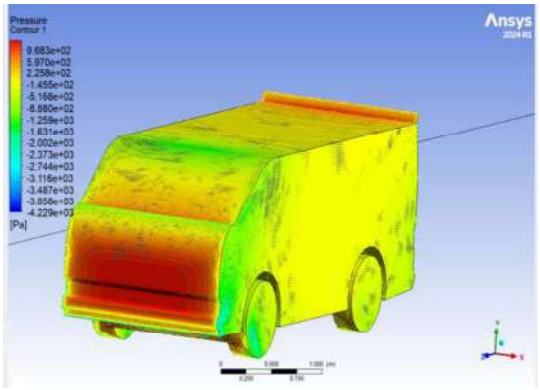


**Fig. 38.** Static pressure

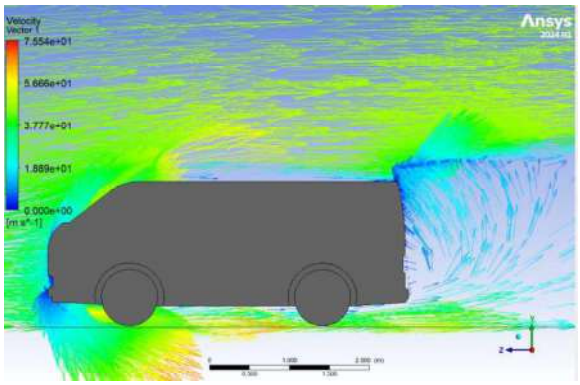


**Fig. 39.** Velocity vector

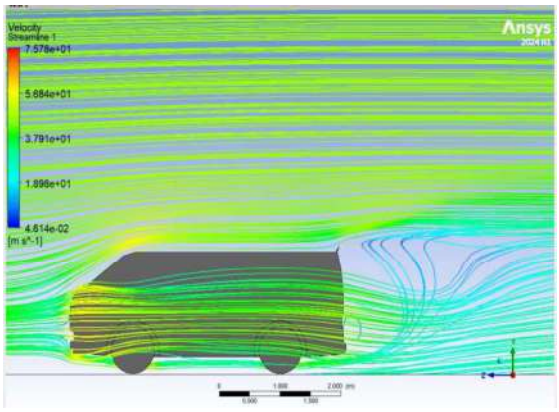


**Fig. 40.** Velocity streamlines

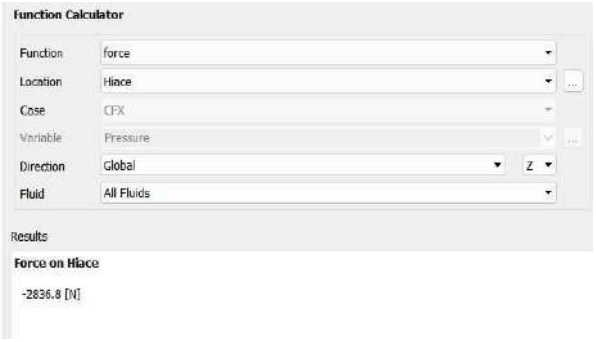


**Fig. 41.** Numerical drag force

The numerical drag force of the optimized Hiace model at 45 m/s is shown in Fig. 41. Similarly, the numerical drag force of the optimized Hiace model at 45 m/s is shown in Fig. 42.


**Fig. 42.** Numerical lift force of the optimized Hiace model at 45 m/s

At a speed of $V = 180\ km/h$ $(50\ m/s)$:

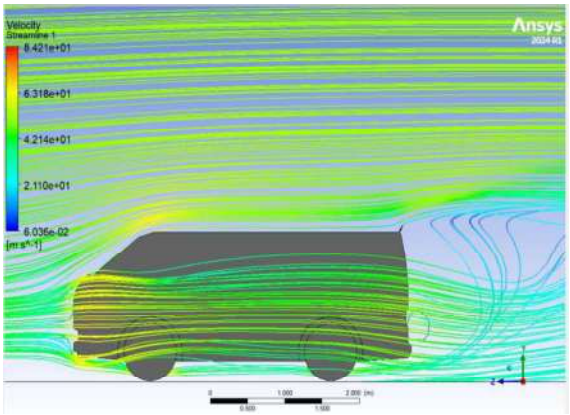


**Fig. 43.** Velocity streamlines

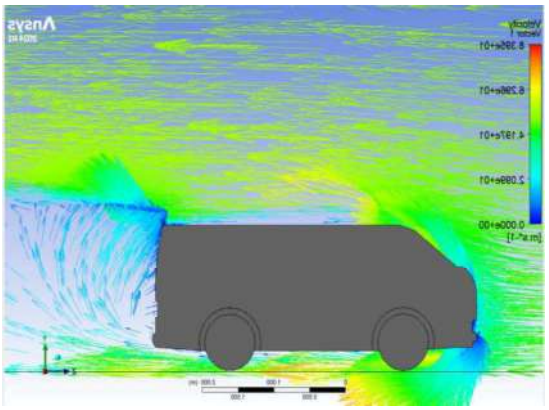

**Fig. 44.** Velocity vector

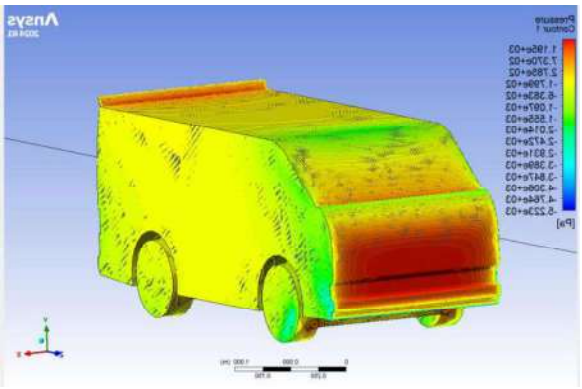

**Fig. 45.** Static pressure


**Fig. 46.** Numerical drag force

The numerical drag force of the optimized Hiace model at 50 m/s is shown in Fig. 46.

Similarly, the numerical drag force of the optimized Hiace model at 50 m/s is shown in Fig. 47.


**Fig. 47**. Numerical lift force of the optimized Hiace model at 50 m/s

Similarly, the numerical values of the drag and lift forces were also applied to Eqs. (1) – (4) to get the numerical drag and lift coefficients, respectively for the optimized Toyota Hiace model.

Table 3 shows the summary of the results from Figs. 33 – 47.

**Table 3.** Aerodynamic Properties of the Optimized Toyota Hiace Model

| **Speed (m/s)** | **Optimized Drag Coefficient $(C_D)$** | **Optimized Lift Coefficient $(C_L)$** | **Optimized Drag Force, $(F_D)$ (N)** | **Optimized Lift Force $(F_L)$ (N)** | **Optimized Maximum Static Pressure $(Pa)$** | **Optimized Maximum Velocity Streamline $(m/s)$** |
|---|---|---|---|---|---|---|
| 40 | 0.7487 | 0.5402 | -2241.18 | -1617.08 | 765.2 | 67.33 |
| 45 | 0.7488 | 0.5410 | -2836.80 | -2049.52 | 968.3 | 75.78 |
| 50 | 0.7488 | 0.5412 | -3502.44 | -2531.44 | 1195 | 84.21 |

Table 3 was used in getting Figs. 48 – 50.

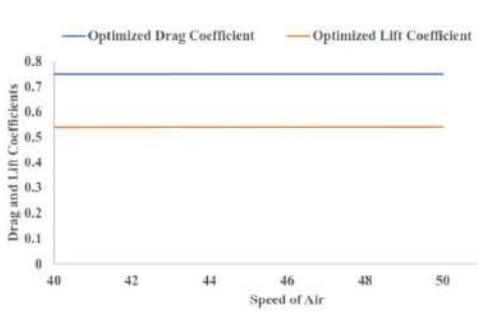


**Fig. 48.** Speed with drag and lift coefficients

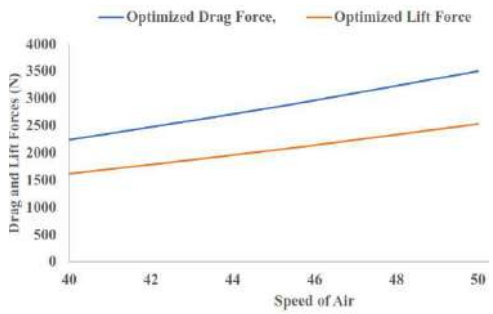


**Fig. 49.** Speed with drag and lift forces

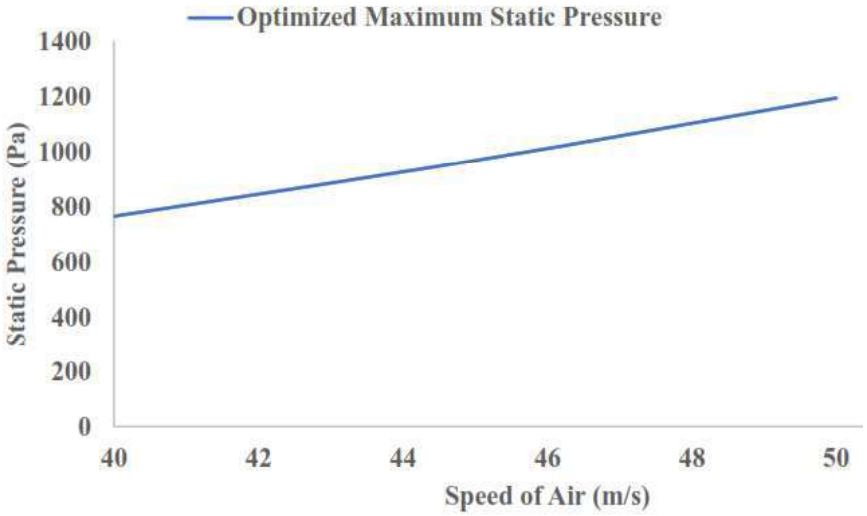


**Fig. 50.** Variation of speed with static pressure in the optimized Hiace model

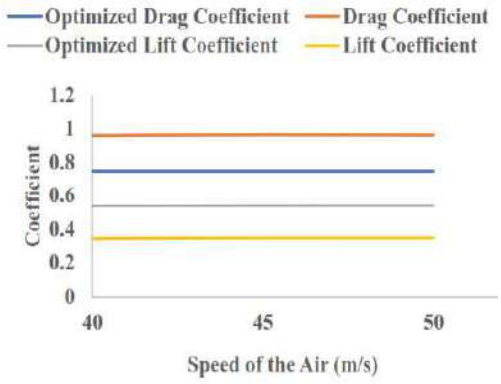


**Fig. 51.** Speed with drag and lift coefficients

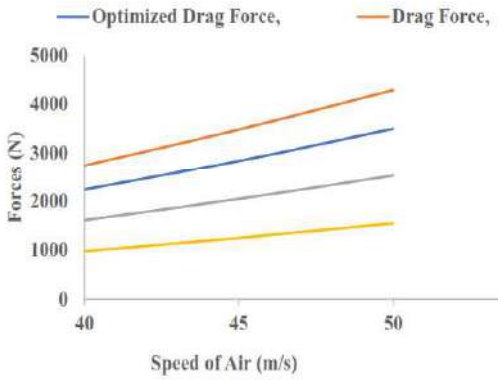


**Fig. 52.** Speed with drag and lift forces

**Table 4.** Comparison of the Drag and Lift Coefficient of the Conventional Hiace Model and the Optimized One

| Speed (m/s) | Optimized Drag Coefficient ($C_D$) | Drag Coefficient ($C_D$) | Optimized Lift Coefficient ($C_L$) | Lift Coefficient ($C_L$) | % Reduction in Drag Coefficient | % Increase in Lift Coefficient |
|---|---|---|---|---|---|---|
| 40 | 0.7487 | 0.9631 | 0.5402 | 0.3443 | 22.26 | 56.90 |
| 45 | 0.7488 | 0.9674 | 0.5410 | 0.3480 | 22.60 | 55.46 |
| 50 | 0.7488 | 0.9656 | 0.5412 | 0.3486 | 22.45 | 55.19 |

Table 4 shows the comparison of the conventional Hiace model with that of the optimized one.

**Table 5.** Comparison of the Drag and Lift Forces of the Conventional Hiace Model and the Optimized One

| Speed (m/s) | Optimized Drag Force, $(F_D)$ (N) | Drag Force, $(F_D)$ (N) | Optimized Lift Force $(F_L)$ (N) | Lift Force $(F_L)$ (N) | % Reduction in Drag Force | % Increase in Lift Force |
|---|---|---|---|---|---|---|
| 40 | -2241.18 | -2741.77 | -1617.08 | -980.211 | 18.26 | 64.97 |
| 45 | -2836.80 | -3485.47 | -2049.52 | -1253.95 | 18.61 | 63.45 |
| 50 | -3502.44 | -4295.25 | -2531.44 | -1550.71 | 18.45 | 63.24 |

**Table 6.** Comparison of the Static Pressure of the Conventional Hiace Model and the Optimized One

| Speed (m/s) | Optimized Maximum Static Pressure $(Pa)$ | Maximum Static Pressure $(Pa)$ | % Reduction in Static Pressure |
|---|---|---|---|
| 40 | 765.2 | 972.9 | 21.35 |
| 45 | 968.3 | 1230 | 21.28 |
| 50 | 1195 | 1525 | 21.64 |

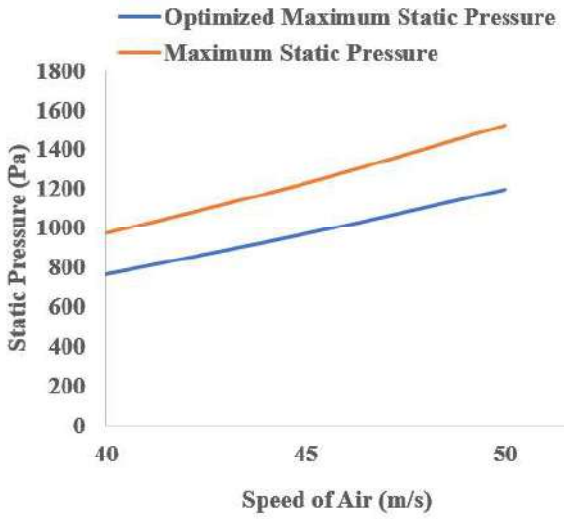


**Fig. 53.** Speed with static pressure in the optimized and conventional Hiace models

From the contour plots, numerical drag and lift forces for the specified wind speeds of 40 m/s, 45 m/s and 50 m/s shown in Figs. 33 – 47, it is seen that the optimized Toyota Hiace model also exhibits higher pressure at its front or nose as the speed of the air in the virtual wind tunnel increases. This is also noted in the numerical drag and lift forces, including the velocity streamlines.

However, the values obtained in the optimized model, except the lift forces and velocity streamlines are lower than that in the conventional one. From the Tables and graphs for the specified wind speeds of 40 m/s, 45 m/s and 50 m/s shown in Tables 4 – 6 and Figs. 48 – 53. It is also seen that the drag and lift coefficients appear to be approximately the same regardless

of the wind speed. This also shows that the drag and lift coefficients are not dependent on the speed of the air. Hence, the optimized Hiace model is expected to have the same drag coefficient ($C_D$) and lift coefficient ($C_L$) at any speed (Johan, 2013) (Fig. 51). Similarly, it is also seen that the drag forces, lift forces, static pressures and velocity streamlines of the optimized model also increases as the wind speed increases despite having lower values apart from the lift forces and velocity streamlines. The addition of the rear spoiler on the rear top of the model helps to minimize turbulence at the rear and drag force while increasing downforce and leading to improved stability. CFD simulations using Shear Stress Transport (SST) equations showed the impact of rear roof spoilers on aerodynamic drag. The results suggest that a simple strip-type spoiler provides beneficial effects when set at a pitch angle of 0° to 7° (Viken et al. 2025). However, an angle of attack (AOA) ($6.75^0$) was used based on the specification of the airfoil. The pressure contour showed how the modification to the rear top of the conventional Toyota Hiace model has redistributed the pressure acting on the front of the car. The highest static pressure on the optimized Toyota Hiace model is 1525 Pa at the highest speed of 50 m/s. This showed a percentage reduction of 21.64 % (Table 6), which is a reduction of 330 Pa when compared to the conventional one. The velocity streamline analyses of the model also revealed a distinctive aerodynamic profile and airflow characteristics. The optimized model also demonstrates a convergence of streamlines along the hood and windshield thereby aligning with Bernoulli's principle and highlighting the aerodynamic wake for in-depth analysis of drag and lift forces. Smoothly curved streamlines over the hood and roof showcase a well-designed aerodynamic profile that minimizes turbulence (Nur and Mohammad, 2024). The CFX analysis shows that the altered area of the conventional model had a positive effect on the overall drag acting on the car. The drag force was drastically reduced by a percentage of 18.45 % (792.81 N) at the highest wind speed of 50 m/s, and the drag coefficient was also reduced by a percentage of 22.45 % (0.2168) from 0.9656 to 0.7488 also at the highest speed.

Specifically, from Tables 4 - 6 and Figs. 51 – 53, it is clearly seen that the optimized Hiace model has outperformed the conventional Hiace model in all the aerodynamics properties. The streamlines in the optimized model show that the airflow over the vehicle after the modifications on the top surface has been affected, as more air is flowing over the top of the car due to the added spoiler. The air flowing over the bonnet is more attached and laminar. The percentage reduction in the drag force, drag coefficient and static pressure in the optimized Hiace model showed that the model can be accepted and recommended for massive production of Toyota Hiace Buses. Most importantly, the increased lift force and lift coefficients are exhibited by the optimized model. A well-optimized aerodynamic design reduces air resistance (drag force), which is one of the most dominant forces acting against a moving vehicle (Viken et al. 2025). The drag force is generated due to the interaction between the car's surface and the surrounding air, and its reduction can lead to substantial fuel savings.

## 4. CONCLUSION

It could be concluded that a CFD of vehicle geometry by reducing drag force in ANSYS was successfully done using the ANSYS 2024 R1 commercial software after modelling the two

models in SolidWorks 2023 software. After the successful analysis, it was observed that the optimized model had a lower drag coefficient, drag forces and static pressures. But gave higher lift coefficients, lift forces and velocity streamlines when compared with the conventional one. The highest static pressure on the optimized Toyota Hiace model was 1525 Pa at the highest speed of 50 m/s. This showed a percentage reduction of 21.64 % when compared to the conventional one. The drag force was drastically reduced by a percentage of 18.45 % (792.81 N) at the highest wind speed of 50 m/s and the drag coefficient was also reduced by a percentage of 22.45 % (0.2168) from 0.9656 to 0.7488, also at the highest speed. Similarly, the lift force was drastically increased by a percentage of 63.24 % (980.73 N) at the highest wind speed of 50 m/s, and the lift coefficient was also increased by a percentage of 55.19 % (0.1926). Hence, following the values obtained from the optimized model would give a better aerodynamic performance, better stability and efficient fuel economy in the model. Hence, recommended for the mass production of Toyota Hiace Buses.

## ACKNOWLEDGEMENTS

We appreciate God almighty. We also acknowledge the Faculty of Engineering, Edo State University, Iyamho for supporting us during this work. Special appreciation goes to our families for their valuable contributions to this research.

## REFERENCES

Ainul, G., Muhamad, A., Made, N. P., Satrio, G. B., Mallory, E., Sonny, S. and Rivaldo, A. (2023). CFD Simulation of Aerodynamics Truck Using Cylinder as Drag Reduction Device. *Journal of Advanced Research in Fluid Mechanics and Thermal Sciences*, 105(2): 166–181.

Arabaci, S. K. and Pakdemirli, M. (2023). Aerodynamic Improvements of Buses Inspired by Beluga Whales. *Journal of Applied Fluid Mechanics*, 16(12): 16-19.

Garg, S. (2019). Study of Various Passive Drag Reduction Techniques on External Vehicle Aerodynamics Performance: CFD Based Approach. *International Research Journal of Engineering and Technology (IRJET)*, 3: 16-21.

Giguere, P. and Selig, M. S. (1997). Low Reynolds Number Airfoils for Small Horizontal Axis Wind Turbines. *Wind Engineering,* 21(6): 367-380.

Heisler, H. (2002). Vehicle body aerodynamics, *Adv. Veh. Technol.,* 4: 584-634, doi: 10.1016/b978-075065131-8/50015-4.

Ikrami, A., Ghani, R. H., Irfan, A., Aieman, S., Khairul, H., Djamal, H. D. and Bukhari, M. (2023). Computational Fluid Dynamics (CFD) Study on The Aerodynamic of Truck. Journal of Design for Sustainable and Environment, 5(2): 23-27.

Isaac, F. O and Abu, L. (2022). Modelling of a Conventional Piston of a Single Cylinder Four-Stroke Diesel Engine by using SolidWorks. *FUOYE J Eng Technol.* 7(1): 65–68.

Johan, B. (2013). Analysis of the aerodynamic attributes of motor vehicles. Bachelor of Engineering (Mechanical) Dissertation, University of Southern Queensland Faculty of Health, Engineering and Sciences, 90 pp.

Muhammad, N. F. K., Izuan, A. I., Nofrizalidris, D., Daniel, S. B. M., Safra, L. S., Razlin, A. R., and Muhamad, A. A. (2021). A Review of Aerodynamics Influence on Various Car Model Geometry through CFD Techniques. *Journal of Advanced Research in Fluid Mechanics and Thermal Sciences*, 88(1): 109–125.

Nath, D. S., Pujari, P. C., Jain, A. and Rastogi, V. (2021). Drag Reduction by Application of Aerodynamic Devices in a Race Car, *Adv. Aerodyn.,* 3(1): 45-51, doi: 10.1186/s42774-020-00054-7.

Nur, I. Z. and Mohammad, K. A. (2024). Aerodynamic Comparison on Different Types of Two-Seater Car Using ANSYS CFX. *Research Progress in Mechanical and Manufacturing Engineering,* 5(1): 662-671.

Qin, P., Ricci, A. and Blocken, B. (2024). CFD simulation of aerodynamic forces on the DrivAer car model: Impact of computational parameters. *Journal of Wind Engineering and Industrial Aerodynamics*, 248: 105-111.

Rutuja, R. K. (2024). Aerodynamic Drag Reduction of Heavy Vehicle Using Computational Fluid Dynamics (CFD). International Journal of Scientific and Research Publications, 14(2): 311-321. https://dx.doi.org/10.29322/IJSRP.14.02.2024.p14634

Velagapudi, N. K., Rao, L. N. V. N. and S. R. Y. (2015). Investigation of Drag and Lift Forces over the Profile of Car with Rear spoiler using CFD, *Int. J. Adv. Sci. Res.,* 1(8): 331-339, doi: 10.7439/ijasr. v1i8.2510.

Viken, B. B., Siddharth, A. S., Karan, M. G. and Devam, S. T. (2025). Shaping the Flow: Aerodynamic Forces, Drag Reduction, and Stability in Modern Vehicles. *International Research Journal of Engineering and Technology (IRJET),* 12(50): 480-498.

**www.airfoiltools.com**

**www.the blue-print.com**

Wendt, J. F. (2009). *Computational Fluid Dynamics*. Springer Berlin Heidelberg. 10.1007/978-3-540-85056-4.